MODELLING HORIZONTALVELOCITIES WITHIN THE WAVE BOTTOM BOUNDARY LAYER

Tiago Abreu [(1)], Paulo A. Silva [(2)], Francisco Sancho [(3)], Hervé Michallet [(4)], Luís Vasconcelos [(1)]

[(1)] CESAM & Department of Civil Engineering, Polytechnic Institute of Viseu, ESTGV Campus de Repeses, 3504-510 Viseu, Portugal. tabreu@estv.ipv.pt, vasconcelos@estv.ipv.pt

[(2)] CESAM & Department of Physics, University of Aveiro, 3810-193 Aveiro, Portugal. psilva@ua.pt

[(3)] LNEC-DHA, National Civil Engineering Laboratory, Av. do Brasil, 101, 1700-066 Lisboa, Portugal. fsancho@lnec.pt

[(4)] LEGI Laboratoire des Ecoulements Géophysiques et Industriels, G-INP/UJF/CNRS, B.P.53, 38041 Grenoble Cedex 9, France. herve.michallet@legi.grenoble inp.fr

ABSTRACT

As waves travel and shoal towards a beach, their surface elevation becomes peaky (sharp crests) and asymmetric relative to the vertical, differing from the sinusoidal profile of linear waves. Below the surface, the passage of the progressive waves induces fluid velocities, showing similar (time) asymmetries. These nonlinearities are inextricably linked to sediment transport, but the processes involved are not well understood. This work analyses the data collected during a recent experimental project under skewed oscillatory flows. It validates a simple method based on the defect law to reproduce the horizontal velocities within the wave bottom boundary layer. Results indicate a good agreement between the measured and modeled velocities using this methodology.

KEY WORDS

Oscillatory flows, horizontal velocities, defect law, sheet-flow.

1. Introduction

Sediment transport is mainly caused by the action of waves or currents or, a combination of both. For increasingly shallow waters, these hydrodynamic processes induce motions on the seabed and if the grains are exposed to large enough velocities they start to move. The processes that intervene in the mechanisms of sediment transport are complex (e.g., forces at mobile beds, sediment-flow interactions) and the scientific community has been engaged in improving our understanding and modelling capabilities. Though several progresses have been made in the past decades, this issue remains a challenge to researchers.

The poor understanding of the processes is partially due to the complexity of the energetic nearshore and to the scarcity of available comprehensive and high quality datasets about detailed sediment transport mechanisms. Also, measurements of the complex sediment-flow interactions and forces still pose challenging technical difficulties. Accurate measurements of the flow velocity in the bottom boundary layer under oscillatory motions require high-end equipments, which usually cannot operate in field conditions. Even in laboratory controlled conditions, this requires sophisticated equipment operation, data protocols and data processing techniques. It is thus desirable to develop theories which allow estimating the velocity in such wave motions.

This work presents a simple method based on the defect law [1] to reproduce the horizontal velocities within the wave bottom boundary layer. The theory is checked against the measured velocity profiles gathered with a high resolution ADVP (Acoustic Doppler Velocity Profiler). The data was collected during a recent experimental project performed at the Large Oscillating Water Tunnel of Deltares under flat-bed/sheet flow conditions, allowing to analyse the effects of wave nonlinearities and of a net current on the sediment transport processes [2, 3, 4].

2. TRANSKEW Experiments

2.1 Experimental Set-up

Intense wave orbital velocities near the bed, occurring typically in the coastal surf zone or even at intermediate water depths during storm conditions, can cause the sand bed to move as a sheet layer, known as sheet flow. This happens for large shear stresses, causing the development of extremely large sediment concentrations and, consequently, high sediment transport rates.

A recent series of experiments to evaluate the net transport rates in sheet flow under oscillatory skewed flows were performed in the Large Oscillating Water Tunnel of Deltares (LOWT) [2,3].

The tunnel has the shape of a U-tube, consisting of a long (14m), rectangular, horizontal section connected to a vertical cylinder at each end (Figure 1). The tunnel was designed for full-scale simulation of the near-bed horizontal oscillating water motion, which can be combined with a steady current. Scale effects, typical of sediment transport studies in smaller laboratory wave flume facilities, are therefore avoided. The desired motion in the test section is created by the movement of the

piston in one of the cylinders. Detailed descriptions of the facility can be found in [5]. In the present experiments, the bottom of the tunnel was covered with a 0.3 m layer of well-sorted sand with a median diameter, $d_{50} \approx 0.20$ mm. Net sediment transport rates and detailed measurements of time-dependent sand concentrations and flow velocities in the suspension and sheet flow layers were determined using various instruments [2,4,6].

For the aim of the present work, one focuses on the velocity time-series collected by an Electromagnetic Flow Meter (EMF), above the wave boundary layer (at approximately 30 cm above the initial bed level), and by an Acoustic Doppler Velocity Profiler [7] located 35 cm above the bed, pointing downwards. The EMF provides information of the measured free-stream horizontal velocities, whereas the acoustic device measures velocity profiles near the bottom and within the entire boundary layer.
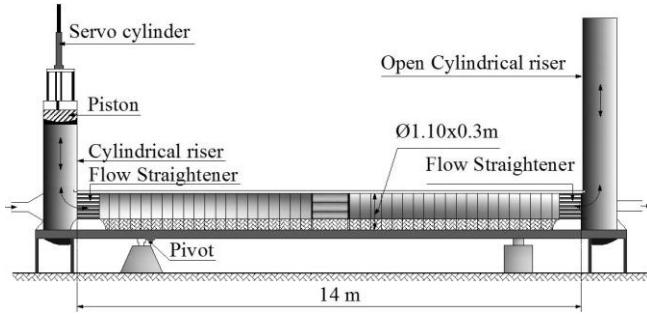

Figure 1. General outline of LOWT

2.2 Test Conditions

The steering signal of the piston has to be formulated in order to reproduce the desired hydraulic conditions in the test section. In the present experiments a regular sawtooth oscillatory flow with different degrees of acceleration skewness was devised (with or without a net current) as well as an oscillatory flow with both velocity and acceleration skewness.

In the experiments a more general expression for velocity- and acceleration-skewed oscillatory flows was developed by [8] and used to drive the LOWT piston, surpassing some limitations of the previous existing formulae. The regular horizontal free-stream velocity, u, is given by the general form:

$$u(t) = U_w f \frac{\left[\sin(\omega t) + \dfrac{r\sin\phi}{1+\sqrt{1-r^2}}\right]}{\left[1 - r\cos(\omega t + \phi)\right]} \qquad (1)$$

where U_w represents the amplitude of the orbital velocity, $U_w = (u_{max} - u_{min})/2$, $\omega = 2\pi/T$ is the angular frequency of a flow period T, and the dimensionless factor $f = \sqrt{1-r^2}$ allows the velocity amplitude to be equal to U_w.

Furthermore, r is an index of skewness or nonlinearity, and ϕ is a waveform parameter related to the biphase (e.g., [9]; [10]). Eq. (1) represents a wide range of nearshore nonlinear wave orbital velocity shapes, depending on the value that the waveform parameter ϕ ($-\pi/2 \leq \phi \leq \pi/2$) takes. A purely acceleration-skewed flow (i.e. sawtooth wave) is obtained for $\phi = 0$ and a pure velocity-skewed flow for $\phi = -\pi/2$. Between these two extreme values the orbital flow contains both velocity and acceleration skewness.

For the particular conditions of combined oscillatory-current flow, a net current, U_0, was added to the oscillatory signal imposed by Eq. (1).

Table 1
Experimental conditions

Condition	U_w (m/s)	U_0 (m/s)	T (s)	r (-)	ϕ (rad)
A1	1.2	0	7	0.30	0
A3	1.2	0	7	0.50	0
C1	1.2	0	7	0.50	-π/4
B2	1.2	-0.4	7	0.30	0
B4	1.2	-0.4	7	0.50	0

Table 1 lists the characteristics of the 5 different test conditions (A1, A3, B2, B4 and C1) that are considered in this work. Series A consisted of regular oscillatory flows with different degrees of acceleration skewness; series B considered acceleration-skewed oscillatory flows with a collinear net current (U_0), opposing the (implied) wave direction; and series C involved a condition with both velocity- and acceleration-skewness.

Figure 2 plots the free-stream velocity, u, for tests A1, A3 and C1, using Eq. (1). The differences between the shapes of u are due to differences between the values of r and ϕ.
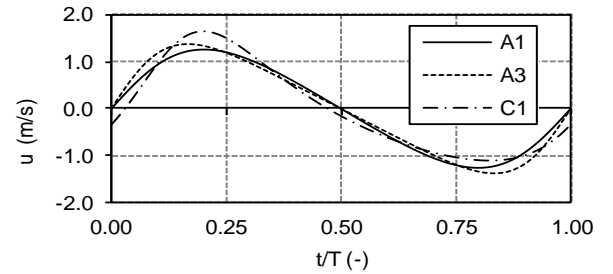

Figure 2. Free-stream velocity for tests A1, A3 and C1

2.3 Velocity Measurements

Detailed velocity measurements within the bottom boundary layer were obtained with a high resolution Acoustic Doppler Velocity meter Profiler (ADVP). The device provides detailed velocity measurements from approximately 150 mm above the bed to within the sheet flow layer [7]. It is composed of a sensor emitting at

2 MHz and two receivers positioned at the same depth (in this experiment about 35 cm above the bed) and 7.9 cm to the centre of the emitter (Figure 3). The acoustic pulse is repeated at 1.6 kHz. The phase shift of the backscattered acoustic signal is recorded every 4 μs. This enables to deduce velocities along the receivers beam axis over a whole profile with a vertical resolution of about 3 mm, leading to an equivalent acquisition frequency of 50 Hz.
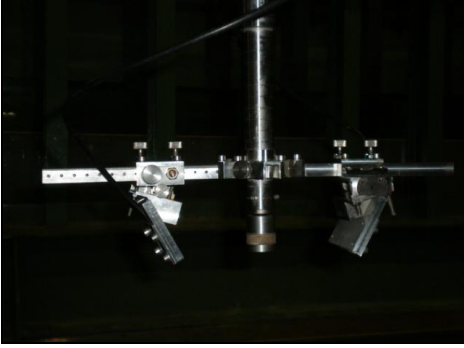

Figure 3. Acoustic Doppler Velocity meter Profiler

From the available number of flow cycles, N_c (≈ 36), the instantaneous velocity obtained with the ADVP were converted in to phase-averaged velocities, $\hat{u}$, according to:

$$\hat{u}(z,t)=\frac{1}{N_c}\sum_{n=1}^{N_c}u\big(z,t+(n-1)T\big), 0\leq t<T ,\qquad(2)$$

where N_c represents the number of flow cycles. The vertical coordinate denoted z is positive upward and $z = 0$ is defined as the initial bed level at the beginning of the experiments, prior to wave action. Figure 4 and Figure 5 show results of the phase-averaged velocities for the oscillatory flow conditions A3 and B4, respectively. At the reference level $z = 0$ the flow does not present velocities equal to zero. This is due to the development of the sheet flow layer structure that mobilizes fluid and particles at lower levels. In addition, during each experiment, there were some small bed level changes of the order of a few millimetres that were accounted for in the ADVP post processing.

The figures provide a good insight of the vertical structure of $u(z)$. The results exhibit typical features of the oscillatory bottom boundary layer: the velocity magnitude first increases with distance from the bed, with an overshoot velocity within the range $z = 10$-30 mm from the bed and, near the bottom, the velocity time series lead the free-stream velocity in phase. In addition, the influence of the acceleration skewness (test A3) leads to a stronger overshoot velocity and a thinner boundary layer under the positive (onshore) velocities.

The comparison of the velocity time series at the upper level ($z = 140$ mm) obtained with the ADVP and with the EMF ($z = 300$ mm), shows that the test without a counter current (Figure 4) presents some mismatches around flow reversal. This is probably due to the low

seeding in the upper part ($z > 3$ cm), during part of the wave cycle [4], affecting the ADVP measurements.

The top panel of Figure 5 also plots the mean horizontal velocity profile, $\bar{u}(z)$, for test B4 (black solid line). The results indicate that the counter current increases from the bottom reaching the free-stream value of U_0 at approximately $z = 80 \sim 90$ mm.
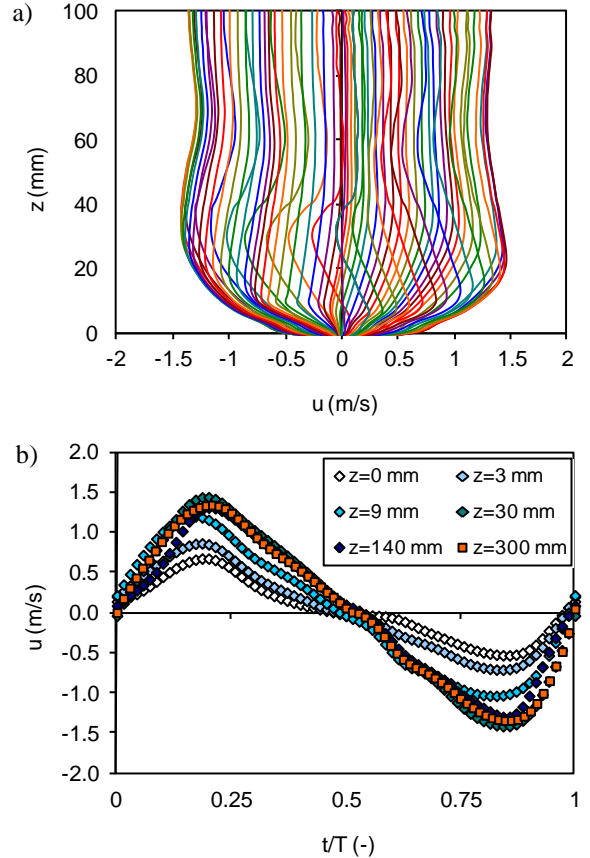

Figure 4. Test A3. a) Phase-averaged velocity profiles; b) Velocity time series at $z = 0, 3, 9, 140$ mm (ADVP) and at 300 mm (EMF)

3. Defect Law

Following [1], the velocities $u(z,t)$ inside the wave bottom boundary layer can be written in terms of the free-stream velocity, $u_\infty(t)$, and a velocity defect $u_d(z,t)$: $u(z,t) = u_\infty(t) - u_d(z,t)$. This equation can be written in terms of a dimensionless velocity defect complex function $D_1(z)$:

$$u(z,t)=\big(1-D_1(z)\big)u_\infty(t)\qquad(3)$$

For laminar oscillatory flows it can be deduced ([1]) that:

$$D_1(z) = \exp\left(-(1+i)\frac{z}{\sqrt{2\nu/\omega}}\right), \qquad (4)$$

where ν is the kinematic viscosity and i is the imaginary unit of complex numbers.
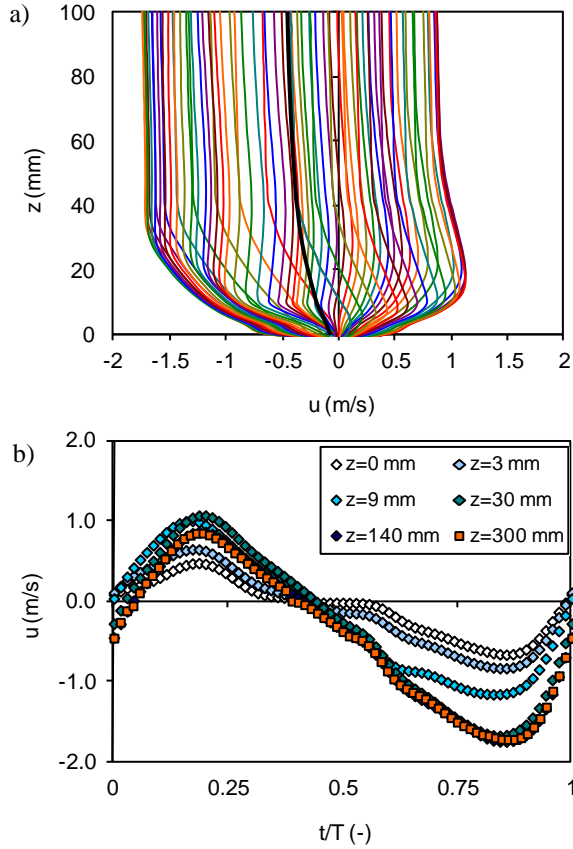
a)

b)

Figure 5. Test B4. a) Phase-averaged velocity profiles; b) Velocity time series at $z = 0$, 3, 9, 140 mm (ADVP) and at 300 mm (EMF)

Eq. (4) implies that the vertical scale of the laminar oscillatory flow is the Stokes length $\sqrt{2\nu/\omega}$. For turbulent flows, [1] suggests that a similar expression can be used:

$$D_1(z) = \exp\left(-(1+i)\left(\frac{z}{z_1}\right)^{p_1}\right) \qquad (5)$$

which reduces to Eq. (4) for $p_1 = 1$ and $z_1 = \sqrt{2\nu/\omega}$. Hence, z_1 represents the velocity decay length scale, whereas p_1 is associated to the velocity gradients. For example, smaller values of p_1 imply larger velocity gradients and, consequently, enhanced bed shear stress. The parameters z_1 and p_1 are derived from an analysis of the primary harmonic of the velocity records.

It is noticed that if z_1 and p_1 adjust well the data, it means that the vertical velocity profile can be estimated

with somewhat reduced information. They allow to obtain $D_1(z)$, which combined with $u_\infty(t)$, provide values for $u(z,t)$ through Eq. (3) (e.g., [11]). In addition, the velocity gradients resulting from this process can be used to assess bed shear stresses.

To obtain z_1 and p_1 the measured velocities $u(z,t)$ are decomposed in a Fourier series:

$$u(z,t) = \frac{a_0(z)}{2} + \sum_{n=1}^{+\infty}\left(a_n(z)\cos(n\omega t) + b_n(z)\sin(n\omega t)\right) \quad (6)$$

where n represents the rank of the harmonics ($n = 1$ corresponds to the fundamental component) and a_n and b_n are the Fourier coefficients. Then, the first harmonic coefficients a_1 and b_1 are computed:

$$a_1(z) = \frac{2}{N_p}\sum_{j=1}^{N_p}\hat{u}\left(z, j\frac{T}{N_p}\right)\cos\left(\omega j\frac{T}{N_p}\right), \qquad (7)$$

$$b_1(z) = \frac{2}{N_p}\sum_{j=1}^{N_p}\hat{u}\left(z, j\frac{T}{N_p}\right)\sin\left(\omega j\frac{T}{N_p}\right), \qquad (8)$$

and are converted to magnitude, r_1, and phase coefficients, ϕ_1:

$$r_1(z) = \sqrt{a_1^2(z) + b_1^2(z)}, \qquad (9)$$

$$\phi_1(z) = \tan^{-1}\left(b_1(z)/a_1(z)\right). \qquad (10)$$

These coefficients are directly linked to the real and imaginary parts of $D_1(z)$ (see Figure 6).
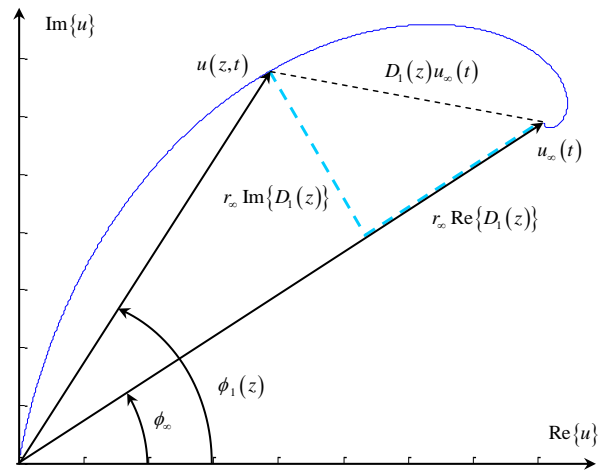

Figure 6. Visualisation of $u(z,t)$ in the complex plane

Figure 6 schematises the result of Eq. (3) in which $u(z,t)$ is constructed geometrically in the complex plane [1]. The solution gives a spiral that starts at the origin of the coordinates, corresponding to the bed where the velocity is zero, and ends at the free-stream velocity, where the distance to the origin equals the amplitude of u_∞. The free-

stream velocity and a generic point $u(z,t)$ are represented as rotating vectors in the complex plane. For a certain elevation z, the module of the vector $u(z,t)$ represents the velocity amplitude and $\phi_1 - \phi_\infty$ correspond to the differences in phase between $u(z,t)$ and $u_\infty(t)$. The values of these phase differences, $\phi_u(z)$, can be calculated from $D_1(z)$:

$$\phi_u(z) = \phi_1(z) - \phi_\infty = \tan^{-1}\left(\frac{\mathrm{Im}\{D_1(z)\}}{1 - \mathrm{Re}\{D_1(z)\}}\right). \quad (11)$$

The real and imaginary parts of $D_1(z)$ can be rewritten as:

$$\mathrm{Re}\{D_1(z)\} = \sqrt{|D_1(z)|^2 - \mathrm{Im}\{D_1(z)\}^2}, \quad (12)$$

$$\mathrm{Im}\{D_1(z)\} = \frac{|D_1(z)|}{\sqrt{1 + \dfrac{1}{\tan^2\left(-A\mathrm{rg}\{D_1(z)\}\right)}}}, \quad (13)$$

with $ln|D_1(z)|$ and $\mathrm{Arg}\{D_1(z)\}$ derived from the measurements, the two parameters z_1 and p_1 are derived as shown in Figure 7.
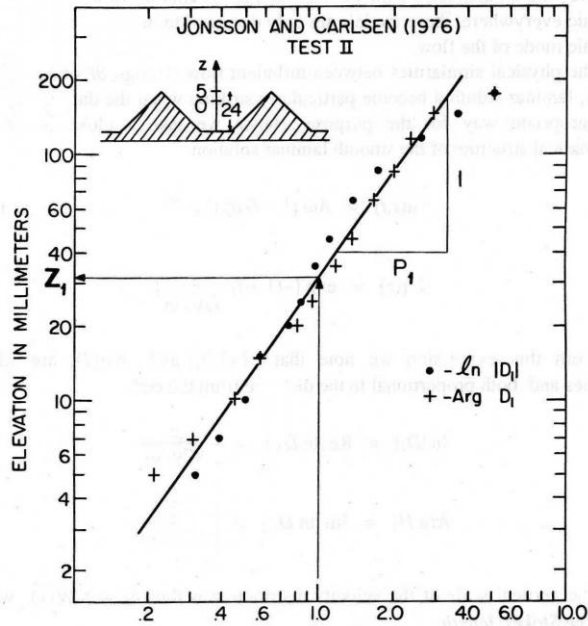

Figure 7. $-ln|D_1(z)|$ and $-\mathrm{Arg}\{D_1(z)\}$ derived from the measurements of [12]. The corresponding values of z_1 and p_1 are determined from the straight line on log-log (adapted from [1])

4. Results

A first harmonic analysis was obtained from the ADVP detailed measurements, providing good insights of the oscillatory boundary layer structure of the flows. Figure 8 exemplifies the vertical structure of r_1 / r_∞ and ϕ_u for tests A3 and B2 (see Eq.s (9) and (11)). The first column evidences that the local velocity amplitude (r_1) increases from the bed and oscillates as a dampened wave around the free-stream value (r_∞) for higher elevations. At about $z \approx 30$ mm the overshoot velocity is reached, leading to $r_1 / r_\infty = 1.14$ and 1.06 for A3 and B2, correspondingly.

The second column of Figure 8 shows a positive phase lead ϕ_u from 0 at $z > 30$ mm, peaking to values of approximately 15º at $z = 6$ mm. Bellow $z = 6$ mm the values of ϕ_u reduce to less than 10º for A3 and even to close to 0º for B2 at $z = 0$. These phase leads and differences can also be observed at the upper plots of Figure 4 and Figure 5, evidencing that the 1st harmonic from the defect law method captures immediately these features.

This contrasts with the acceleration-skewed, fixed-bed experiment results of [13] where ϕ_u continuously increases towards the bed. However, other mobile-bed experiments (e.g., [14,15]) and two-phase model simulations (e.g., [16,15]) present similar vertical structures of ϕ_u as those observed in the TRANSKEW experiments. The differences between fixed and mobile-bed experiments may point to an effect to the high near-bed sand concentrations on the flow in the wave boundary layer [15]. Furthermore, the oscillatory flow experiments with superimposed currents of [14] also suggest a stronger reduction in ϕ_u close to the bed. Thus, apparently, the mean-flow further contributes to the stronger reduction in ϕ_u.
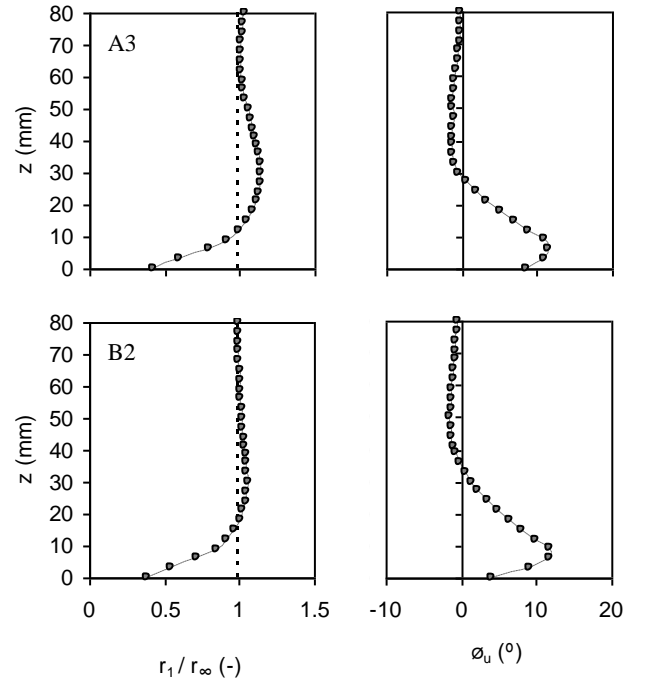

Figure 8. First harmonic analysis for tests A3 and B2. Vertical structure of r_1 / r_∞ and ϕ_u.

Figure 9 plots the vertical evolution of $-ln|D_1(z)|$ and $-\text{Arg}\{D_1(z)\}$ on a log-log scale for the five tests. The z origin was replaced, adding 5 mm to all the ADVP levels to account for the presumable location of the non-moving bed [17]. The power p_1 in Eq. (5) relies on the slope of the best straight-line fit of $-ln|D_1(z)|$ (upper panel of Figure 9). The vertical scale z_1 is obtained from $-ln|D_1(z)|=1$. For the overall experiments, one founds that the values of z_1 are within the range 9-10 mm and $p_1 \approx 0.90$. The tests without a counter current (A1, A3 and C1) have some mismatches in the upper part ($z > 30$ mm) regarding the fitting to a straight-line, which might be attributed to the low suspended concentrations during parts of the flow cycle [4].
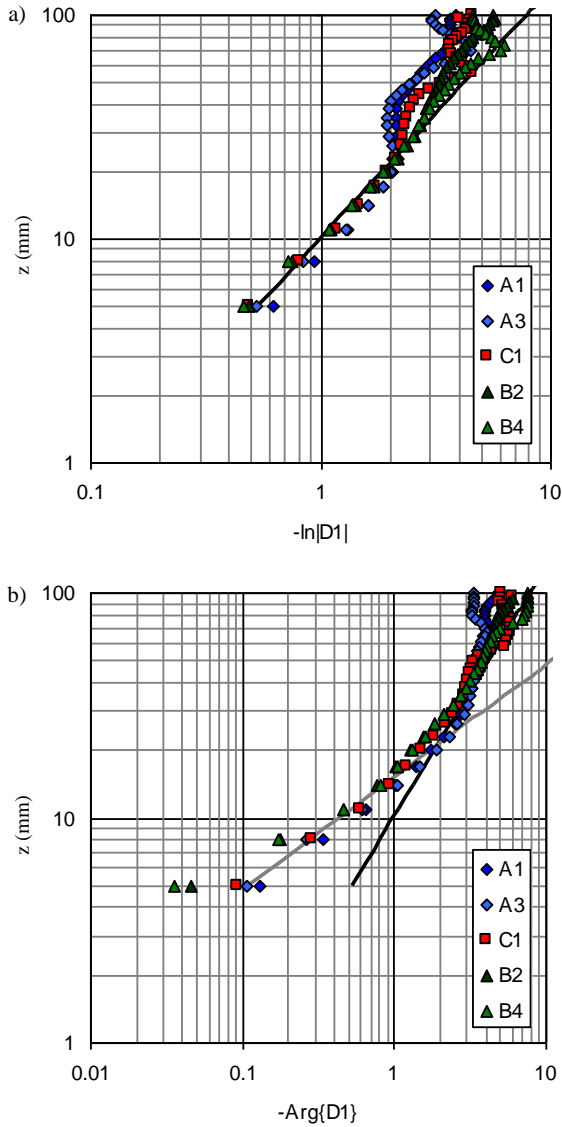

a)

b)

Figure 9. Vertical evolution of $-ln|D_1(z)|$ and $-\text{Arg}\{D_1(z)\}$ for the five test conditions. The continuous lines refer to Eq.s (13) and (14)

Moreover, it is possible to observe in the lower panel of Figure 9 that for higher elevations (> 20 mm) $-\text{Arg}\{D_1(z)\}$ follow quite reasonably the linear trend found for $-ln|D_1(z)|$ (black line). This agrees with [1] observations, where the structure of the turbulent boundary layer is very similar to that of smooth, laminar flow in which the real and imaginary parts of the complex logarithm of the defect function are approximately identical along the water column $(\text{Re}\{ln(D_1(z))\} = \text{Im}\{ln(D_1(z))\})$, or equivalently, $-ln|D_1(z)| = -\text{Arg}\{D_1(z)\}$. Nevertheless, the TRANSKEW experiments reveal some divergence between $ln|D_1(z)|$ and $\text{Arg}\{D_1(z)\}$ at lower elevations and other linear trends could be assumed.

The following expressions represent the continuous lines shown in Figure 9 which roughly approximate the trends of the five flow conditions:

$$|D_1(z)| = e^{-(z/0.010)^{0.90}} \tag{13}$$

$$-\text{Arg}\{D_1(z)\} = \begin{cases} (z/0.010)^{0.90}, z > 0.021m \\ (z/0.015)^{2.0}, z \leq 0.021m \end{cases}. \tag{14}$$

The value of $z = 0.021$ m in Eq. (14) was chosen to obtain the continuity between the two straight-lines with different slopes. Figure 10 plots the vertical evolution of the phase lead ϕ_u using Eq. (11), with the results expressed by Eq.s (13) and (14). Additionally the identity of $\text{Arg}\{D_1(z)\}$ and $ln|D_1(z)|$ is assumed through the use of Eq. (13). The results reveal that the reduction of the phase lead ϕ_u closer to the bed, observed in Figure 8 is recreated when $ln|D_1(z)| \neq \text{Arg}\{D_1(z)\}$. As depicted in Figure 8, B2 presents a stronger decay toward 0 as the bed is approached, suggesting a somewhat lower slope in the second branch of Eq. (14). That can be confirmed in the right panel of Figure 9.
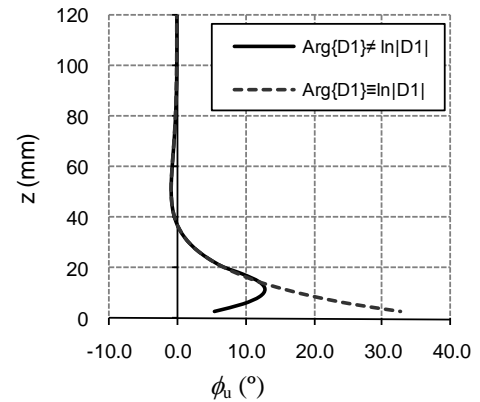

Figure 10. Velocity phase difference, ϕ_u, assuming $ln|D_1(z)| \equiv \text{Arg}\{D_1(z)\}$ and $ln|D_1(z)| \neq \text{Arg}\{D_1(z)\}$

As the vertical structure of the velocity, through $D_1(z)$, was shown to be well defined by Eq.s (13) and (14) with the use of simple parameters (z_1 and p_1), it is possible

to convert them into magnitude and phase coefficients, $r_1(z)$ and $\phi_1(z)$, using Eq.s (12) and (13). This procedure surpasses the incongruent measurements associated with low seeding in the upper part ($z > 3$cm) observed for A1, A3 and C1 during part of the wave cycle. Such information, combined with the EMF free-stream velocity, $u_\infty(t)$, enables the reconstruction of $u(z,t)$. Figures 11 and 12 exemplifies, for tests A3 and B2, the ADVP phase averaged velocities and the predicted velocities according to the defect law analysis. Though the reconstruction relies only on the 1st harmonic component, the results agree fairly well with the ADVP measurements, showing that the defect law reproduces the typical features of the wave boundary layer: (1) the velocity magnitude generally increases with distance from the bed, (2) at different levels the velocities are not in phase, (3) an overshoot of the velocity occurs at a certain elevation (2-4 cm) above the bed.
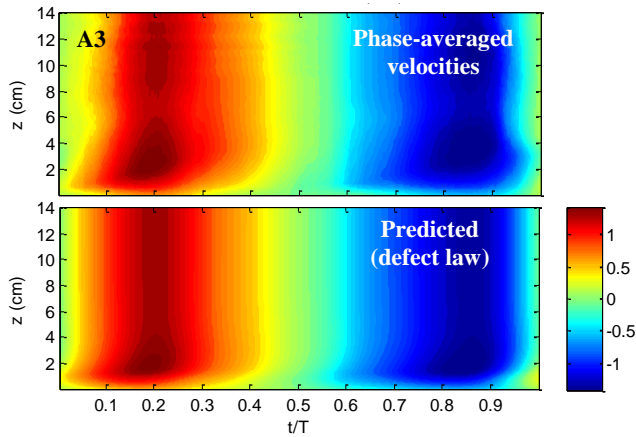

Figure 11. Test A3 – ADVP phase-averaged and predicted velocities (m/s) according to the defect law
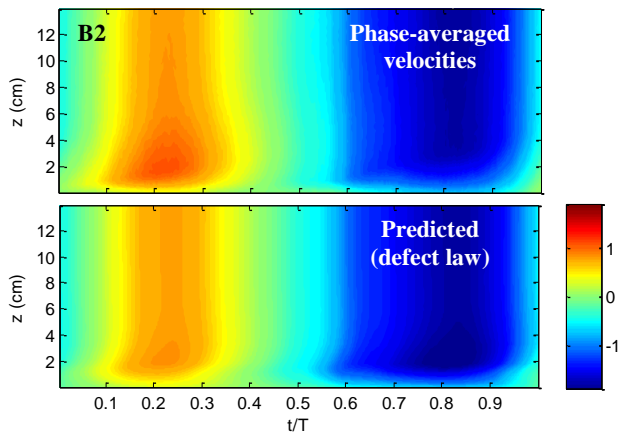

Figure 12. Test B2 – ADVP phase-averaged and predicted velocities (m/s) according to the defect law

5. Conclusion

Detailed measurements of time-dependent flow velocities obtained with a high resolution Acoustic Doppler Velocity meter Profiler allowed the development, application and validation of the defect law, enhancing features of the flow within the boundary layer. The dataset was generated by full-scale, regular, acceleration- and velocity-skewed oscillatory flows combined with opposing net currents, under sheet flow conditions.

The results agree fairly well with the high resolution ADVP measurements and show that the defect law reproduces typical features of the wave boundary layer: (1) the velocity magnitude generally increases with distance from the bed, (2) at different levels the velocities are not in phase, (3) an overshoot of the velocity occurs at a certain elevation (2-4 cm) above the bed.

The consistence of the values suggests that the defect law is verified with the TRANSKEW data and that the use of the defect law can be useful to correct and predict the values where the ADVP failed. In addition, when applied to mobile beds, the methodology replicates the reduction of velocity phase differences, ϕ_u, if different values of z_1 and p_1 are assumed for lower elevations in $\text{Arg}\{D_1(z)\}$. It is noted that, according to [1], the parameters z_1 and p_1 could be prescribed as function of the relative roughness (A/k_s) and the Reynolds number $\left(Re = A^2\omega/\nu\right)$. Therefore, in the future, it would be interesting to investigate such relations in different flow regimes for several experiments. Furthermore, this simple methodology appears promising in many engineering applications that require the knowledge and modelling of the wave boundary layer flow, such as bed shear stresses and sediment transport.

Acknowledgement

References

[1] P. Nielsen, *Coastal Bottom Boundary Layers and Sediment Transport* (Advanced Series on Ocean Engineering, 4, World Scientific, 1992).
[2] P.A. Silva, T. Abreu, D.A. van der A, F. Sancho, B.G. Ruessink, J.J. van der Werf & J.S. Ribberink,

Sediment transport in non-linear skewed oscillatory flows: Transkew experiments, *Journal of Hydraulic Research*, *49*(sup1), 2011, 72-80.

[3] P.A. Silva, T. Abreu, P. Freire, G. Kikkert, H. Michallet, T. O'Donoghue, S. Plecha, J.S. Ribberink, B.G. Ruessink, F. Sancho, K. Steenhauer, A. Temperville, D. van der A & J.J. van der Werf, Sand transport induced by acceleration-skewed waves and currents – The TRANSKEW project, *In: A.J.S.A. Lane (Editor), PECS08 – Physics of Estuaries and Coastal Seas*, Liverpool, UK, 2008, 163-166.

[4] B.G. Ruessink, H. Michallet, T. Abreu, F. Sancho, D.A. van der A, J.J. van der Werf & P.A. Silva, Observations of velocities, sand concentrations, and fluxes under velocity-asymmetric oscillatory flows, *Journal of Geophysical Research*, *116*(C3): C03004, 2011.

[5] J.S. Ribberink & A.A. Al-Salem, Sediment transport in oscillatory boundary layers in cases of rippled beds and sheet flow, *Journal of Geophysical Research*, *99*(C6), 1994, 12707-12727.

[6] T. Abreu, P.A. Silva & F. Sancho, Comparison of sediment transport formulae regarding accelerated skewed waves, *Proc. 31st International Conference on Coastal Engineering*, *Poster Proc.*, Hamburg, Germany, 2008, 145-155.

[7] D. Hurther & U. Lemmin, A Correction Method for Turbulence Measurements with a 3D Acoustic Doppler Velocity Profiler, *Journal of Atmospheric and Oceanic Technology*, *18*(3), 2001, 446-458.

[8] T. Abreu, P.A. Silva, F. Sancho & A. Temperville, Analytical approximate wave form for asymmetric waves, *Coastal Engineering*, *57*(7), 2010, 656-667.

[9] S. Elgar & R.T. Guza, Observations of bispectra of shoaling surface gravity waves, *Journal of Fluid Mechanics*, *161*, 1985, 425-448.

[10] I.A. Leykin, M.A. Donelan, R.H. Mellen & D.J. McLaughlin, Asymmetry of wind waves studied in a laboratory tank, *Nonlinear Processes in Geophysics*, *2*(3/4), 1995, 280-289.

[11] T. Abreu, H. Michallet, P.A. Silva, F. Sancho and P. Nielsen, Velocity defect law in the wave bottom boundary layer, *Proc. 32nd International Conference on Coastal Engineering*, Shangai, China, 2010.

[12] I.G. Jonsson & N.A. Carlsen, Experimental and theoretical investigations in an oscillatory turbulent boundary layer, *Journal of Hydraulic Research*, *14*(1), 1976, 45 - 60.

[13] D.A. van der A, T. O'Donoghue, A.G. Davies & J.S. Ribberink, Effects of acceleration skewness on rough bed oscillatory boundary layer flow, *Proc. 31st International Conference on Coastal Engineering*, Hamburg, Germany, 2008, 1583-1595.

[14] S.R. McLean, J.S. Ribberink, C.M. Dohmen-Janssen & W.N.M. Hassan, Sand Transport in Oscillatory Sheet Flow with Mean Current, *Journal of Waterway, Port, Coastal and Ocean Engineering*, *127*(3), 2001, 141-151.

[15] J. Malarkey, S. Pan, M. Li, T. O'Donoghue, A.G. Davies & B.A. O'Connor, Modelling and observation of oscillatory sheet-flow sediment transport, *Ocean Engineering*, *36*(11), 2009, 873-890.

[16] P. Dong & K. Zhang, Intense near-bed sediment motions in waves and currents, *Coastal Engineering*, *45*(2), 2002, 75-87.

[17] T. Abreu, M.J. Franca, P.A. Silva & F. Sancho, Estimation of sediment particle velocities in sheet flow: cross-correlation and wavelet analysis, *Proc. 6th River Coastal and Estuarine Morphodynamics*, Santa Fe, Argentina, 2009, 1051-1056.